Dense optical storage with phase-change materials

Dr. Juen-Kai Wang, CCMS, NTU

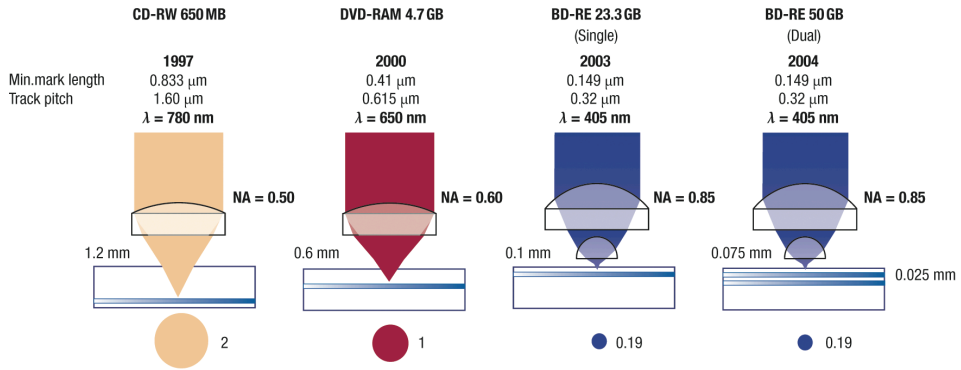

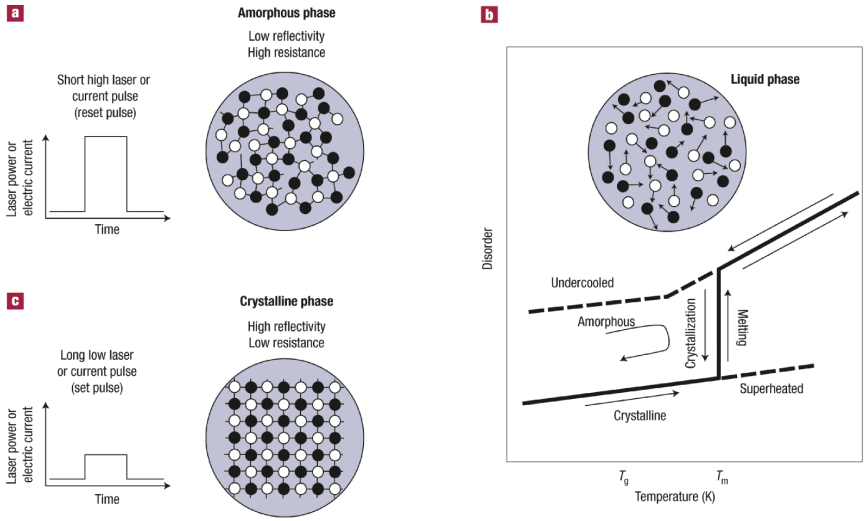

- Blue-ray recordable and erasable discs (BD-RE) is the most advanced commercial optical storage product that provides a single-layer repetitively recordable capacity of 25 GB .
- Phase-change materials, greatly used in optical storage media (such as BD-RE), exhibit reversible switching behavior in optical reflectivity between amorphous and crystalline states created by local laser heating.

M. Wuttig and N. Yamada, Nature Mater. 6, 824 (2007).

TEM examination of blue-ray discs

Dr. Juen-Kai Wang, CCMS, NTU

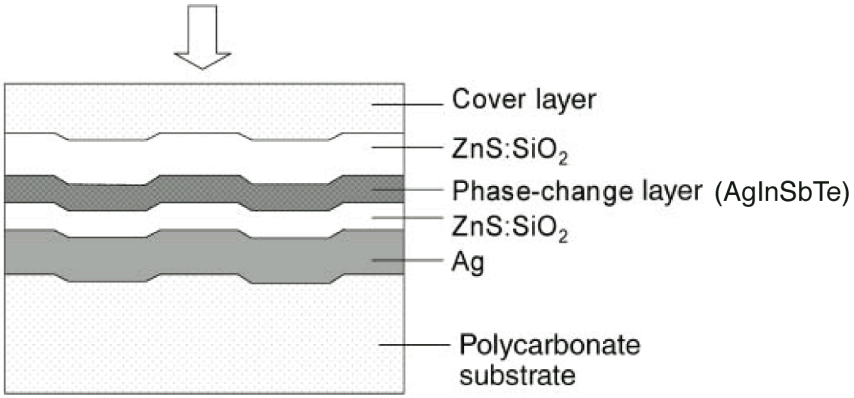

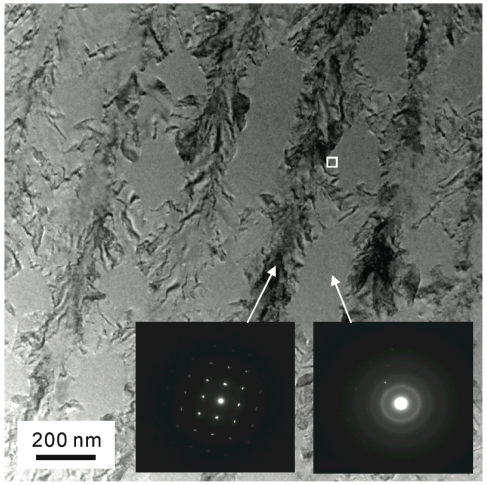

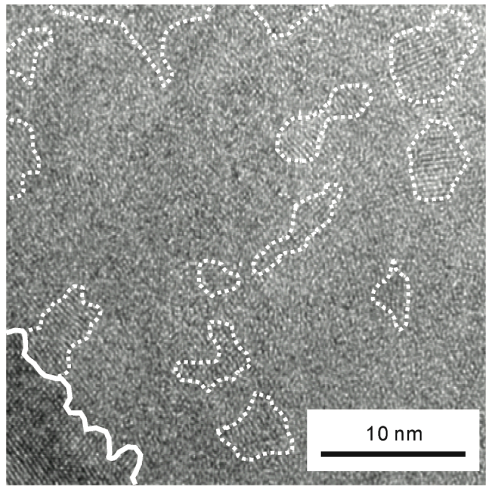

- Blur marks, emerging in the TEM image, represent amorphous regions created by local laser heating.
- Nano-domains with atomic order are barely recognizable in the zoom-in view of the TEM image, because the transmitted electrons have accumulated the influence along the thickness of the recording layer that contains both crystalline and amorphous regions.
- Conductive AFM studies also presented only nonconducting state in the recorded marks, because the isolated crystalline domains do not have a sufficient quantity to provide a percolation threshold for current conduction.

J. Y. Chu et al., Appl. Phys. Lett 95, 103105 (2009).

Near-field examination of blue-ray discs

Dr. Juen-Kai Wang, CCMS, NTU

Near-field image of non-recorded disc

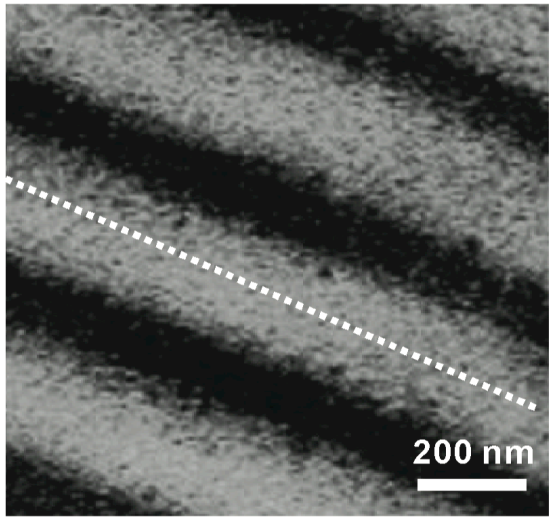

Near-field image of recorded disc

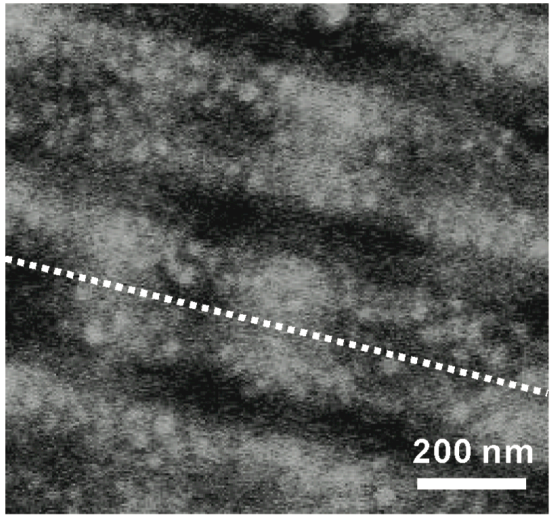

TEM image of recorded mark

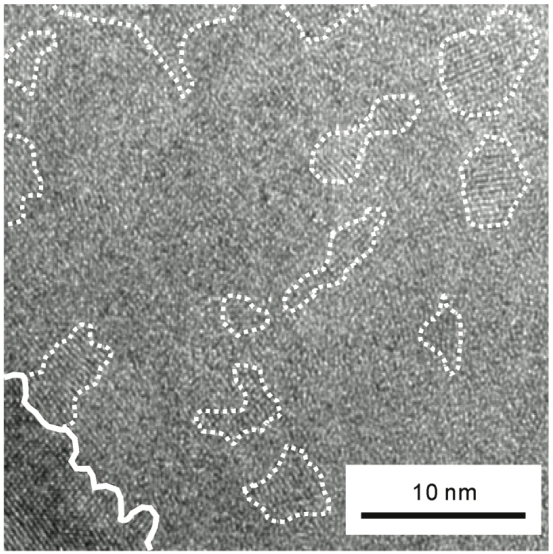

- Darker regions with the comparable size appear in the near-field image. The optical contrasts of the dark region and the bright region are consistent with the calculation based on the optical constants of amorphous and polycrystalline AgInSbTe.
- Small bright spots with a size of ~30 nm emerge within the dark region, corresponding to the nano-sized ordered domains in the TEM image.
- s-SNOM provides a direct optical probe in nanometer scale for high density optical storage media.

J. Y. Chu et al., Appl. Phys. Lett 95, 103105 (2009).

Surface-enhanced Raman scattering

Dr. Juen-Kai Wang, CCMS, NTU

Cross-section (fluorescence) ~ 10^{-16} (cm^2/molecule)
Cross-section (Raman) ~ 10^{-32} (cm^2/molecule)

First Observation of SERS

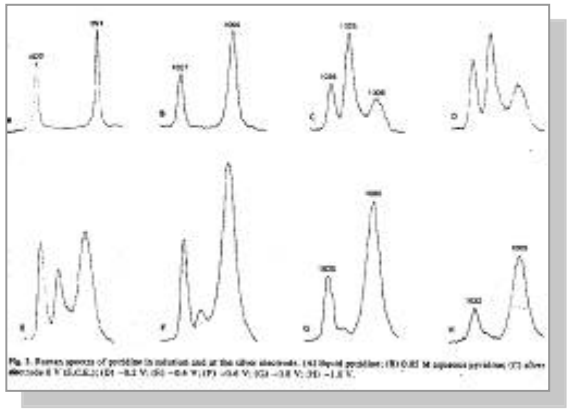

M. Fleishmann et al.,
Chem. Phys. Lett. 26, 163 (1974)

First Direct Observation of 'Hot-Spots' in SERS

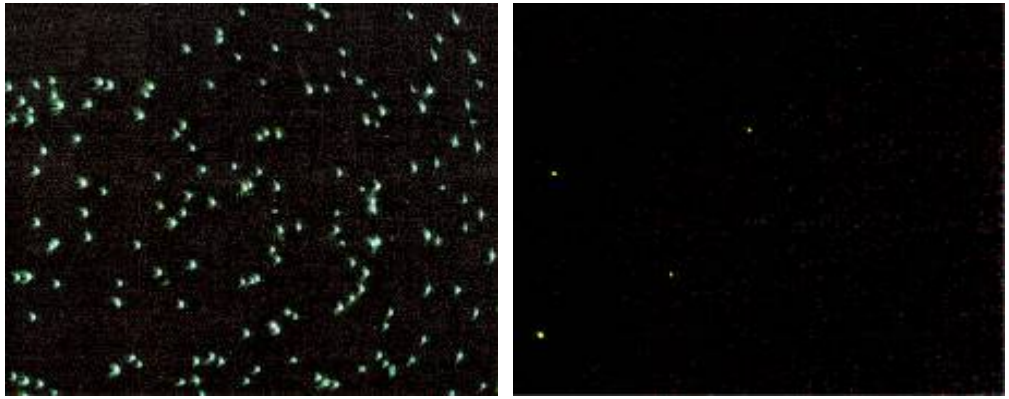

S. Nie and S. R Emory Science 275, 1102 (1997)

- Raman cross-section is ten orders of magnitude less than fluorescence cross-section.
- Exploiting field enhancement to increase Raman signal, facilitating its use in identifying small quantity of chemical and biological species.

Comparison between Raman and SERS

Dr. Juen-Kai Wang, CCMS, NTU

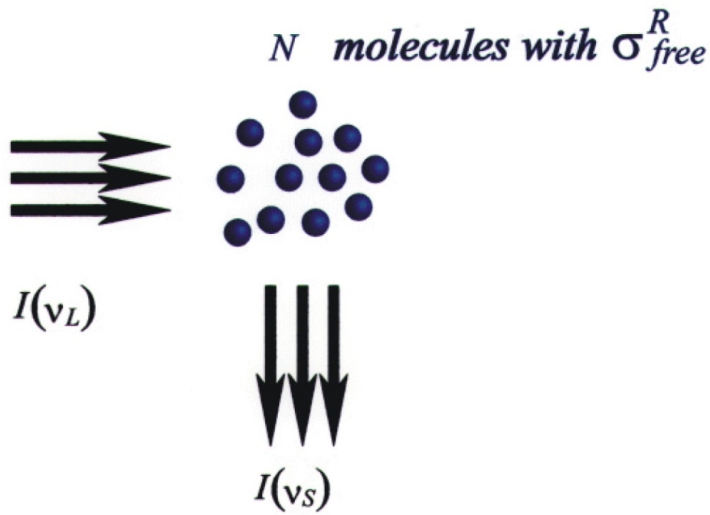

$$I_{NRS}(\nu_S) = N \cdot I(\nu_L) \cdot \sigma^R_{free}$$

Unenhanced Raman scattering

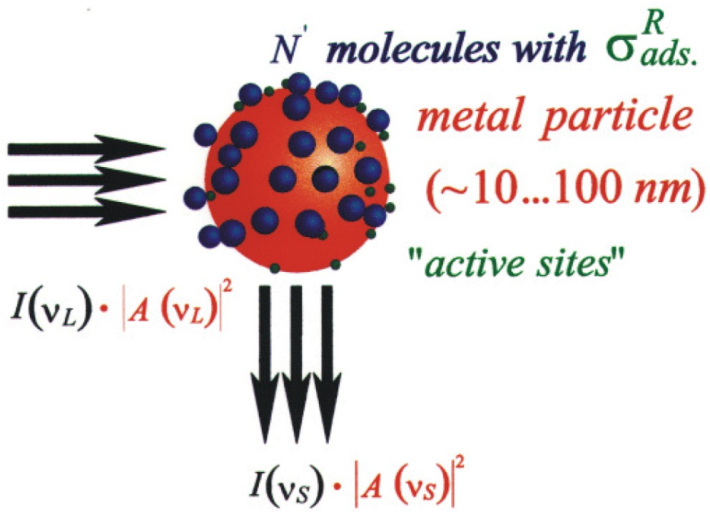

$$I_{SERS}(\nu_S) = N' \cdot I(\nu_L) \cdot |A(\nu_L)|^2 \cdot |A(\nu_S)|^2 \cdot \sigma^R_{ads.}$$

SERS

K. Kneipp et al., Bioimaging 6, 104 (1998).

Effective length scale of SERS

Dr. Juen-Kai Wang, CCMS, NTU

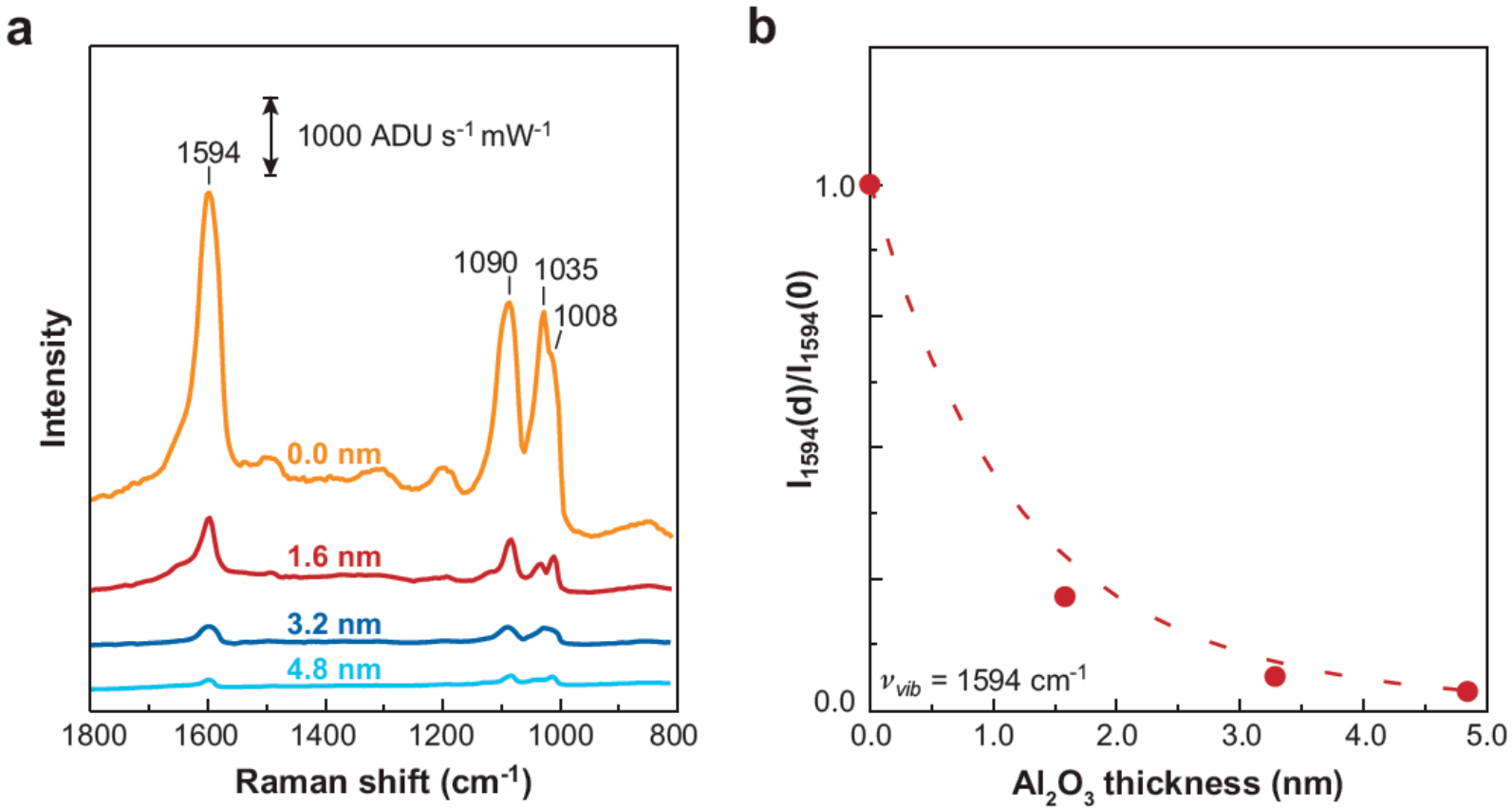

- SERS spectra pyridine adsorbed to silver film over nanosphere samples treated with various thicknesses of alumina.
- Raman signal vs. alumnia thickness is fitted with $I_{SERS} = a^{10}/(a+r)^{10}$.

J. A. Dieringer et al., Faraday Discuss. 132, 9 (2005); D. J. Kennedy et al., J. Phys. Chem. B 103, 3640 (1999).

Interparticle field enhancement in SERS

Dr. Juen-Kai Wang, CCMS, NTU

$$M = \left[E_L(\omega_l)/E_I(\omega_l)\right]^2 \cdot \left[E_L(\omega_S)/E_I(\omega_S)\right]^2$$

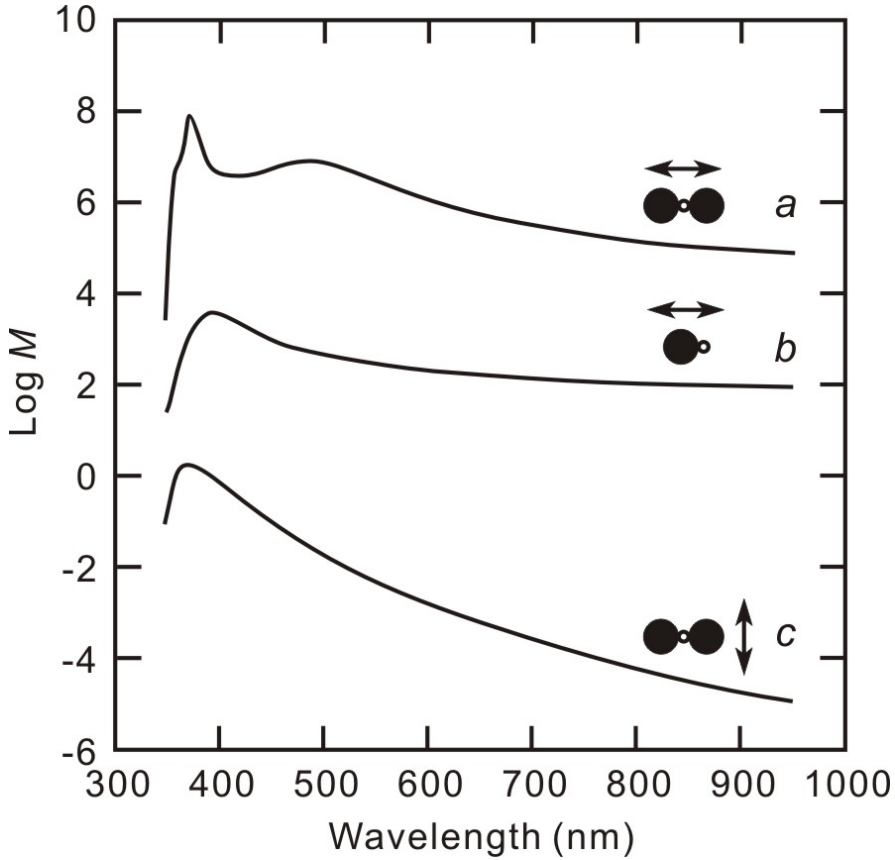

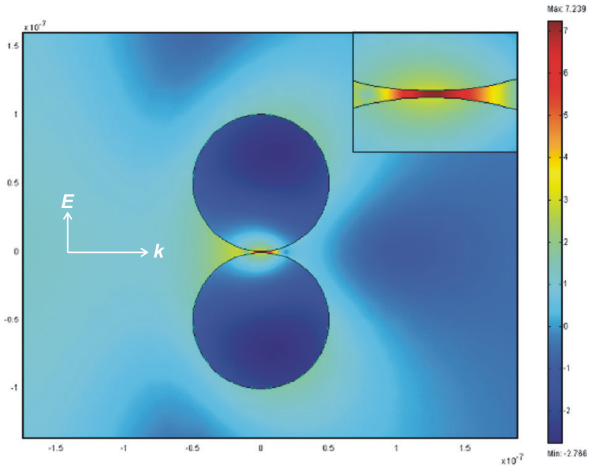

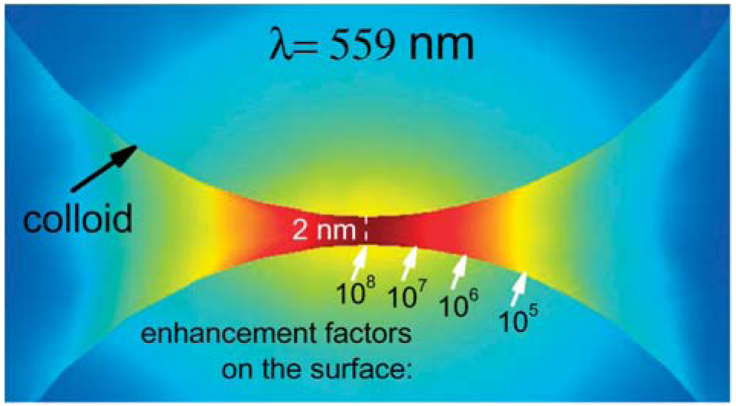

H. Xu et al., Phys. Rev. B 62, 4318 (2000); P. G. Etchegoin and E. C. Le Ru, Phys. Chem. Chem. Phys. 10, 6079 (2008).

Fabrication procedure of Ag-particle arrays

Dr. Juen-Kai Wang, CCMS, NTU

- High-purity aluminum foil is electropolished to 1-nm surface roughness.
- The foil is then anodized using different voltages to obtain arrays of self-organized nanochannels with specific interchannel spacings.
- Identical channel diameter is created by controlled etching for the substrates with different pore spacings.
- By AC electrochemical plating procedure, Ag nanoparticles are grown in the AAO nanochannels.
- The 'hot junctions' are then created by subsequent etching of alumina walls.

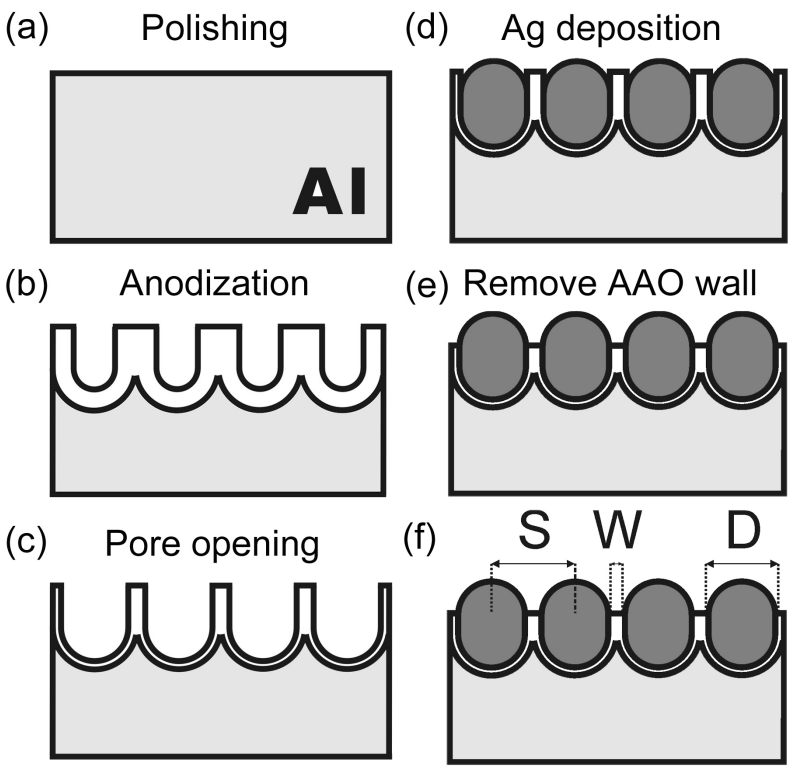

H.-H. Wang et al., Adv. Mater. 18, 491 (2006).

SEM and TEM examination

Dr. Juen-Kai Wang, CCMS, NTU

- The spread of the distribution of *D* and *W* is ~5 nm.
- The hot junctions were further examined by cross-sectional transmission electron microscopy.
- In this study, the gap is tuned from 5 to 25 nm, while maintaining the particle diameter to be 25 nm.

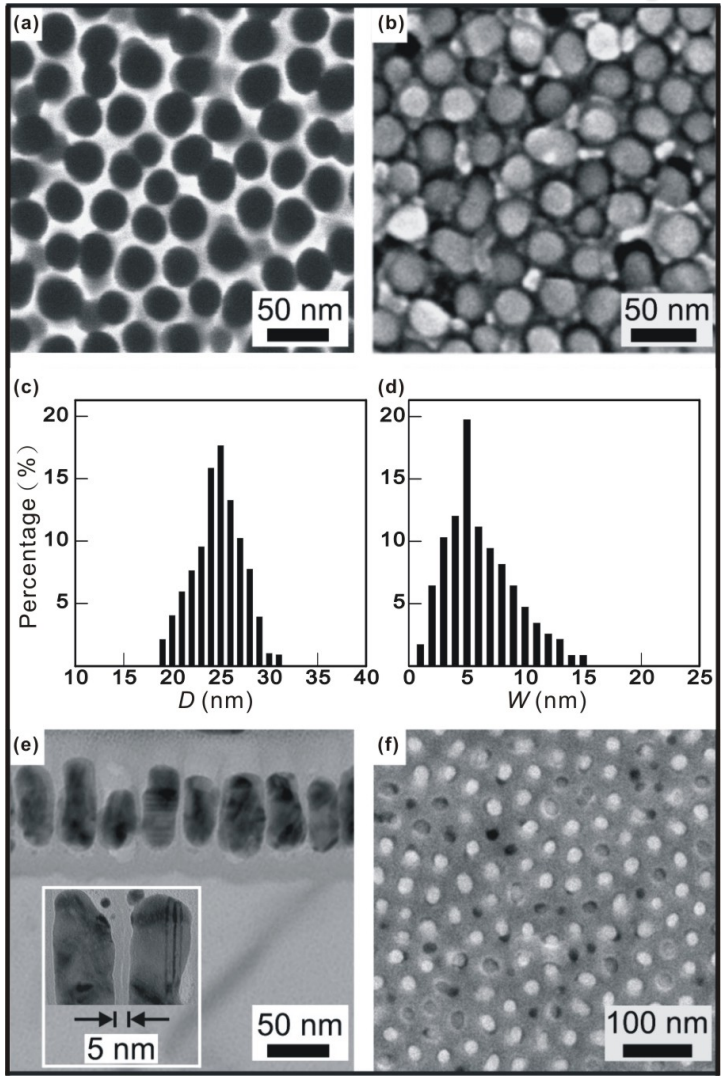

H.-H. Wang et al., Adv. Mater. 18, 491 (2006).

Enhancement & dynamical range

Dr. Juen-Kai Wang, CCMS, NTU

Rhodamine 6G in water

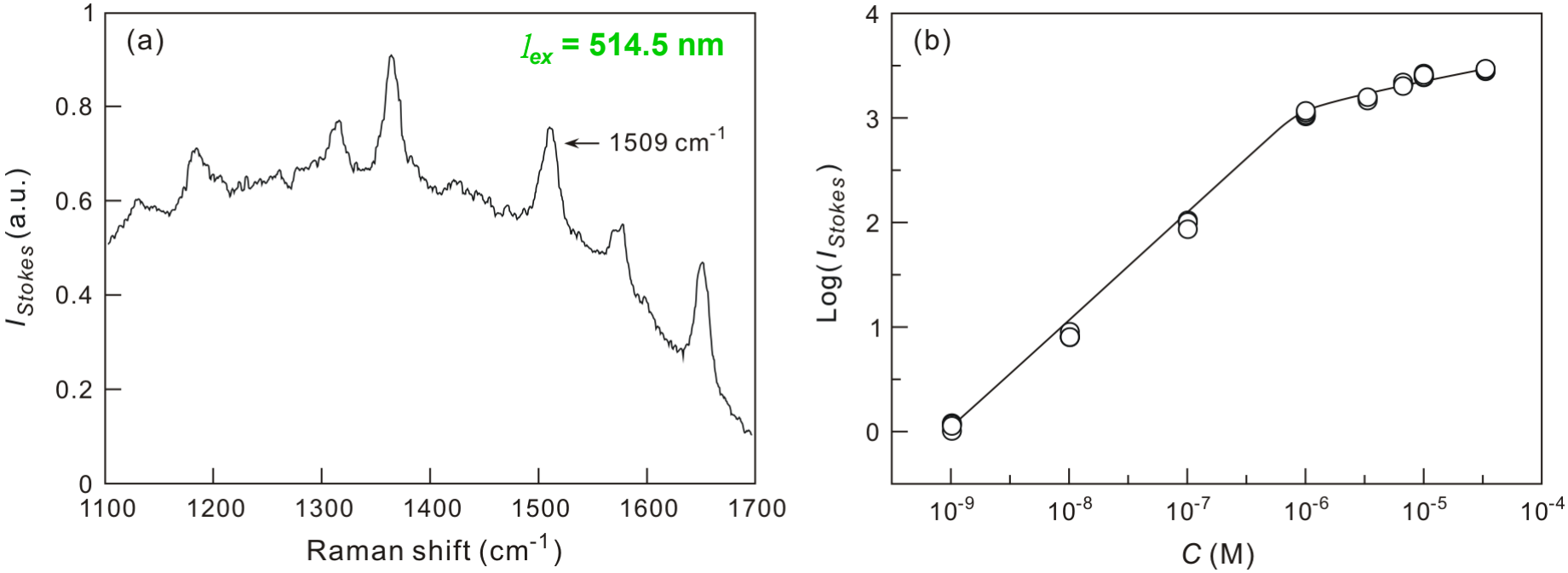

- Uniform Raman enhancement (<5% for different locations of a substrate)
- 10^5 more Raman enhancement than the substrate of ~30 nm Ag nanoparticles thermally deposited on a silicon surface
- Large dynamical range (>1000)

H.-H. Wang et al., Adv. Mater. 18, 491 (2006).

Gap dependence of SERS signal-I

Dr. Juen-Kai Wang, CCMS, NTU

- Adenine: no fluorescence background from 514.5-nm excitation
- 739 cm^{-1}: purine ring breathing mode
- $\hat{I}_{Stokes}$: average Raman signal per particle
- $\hat{I}^{\infty}_{Stokes}$: for substrates with infinitely large *W*
- The average Raman signal per particle at 739 cm^{-1} starts increasing drastically as *W* decreases below 10 nm.

Adenine in water (10^{-4} M)

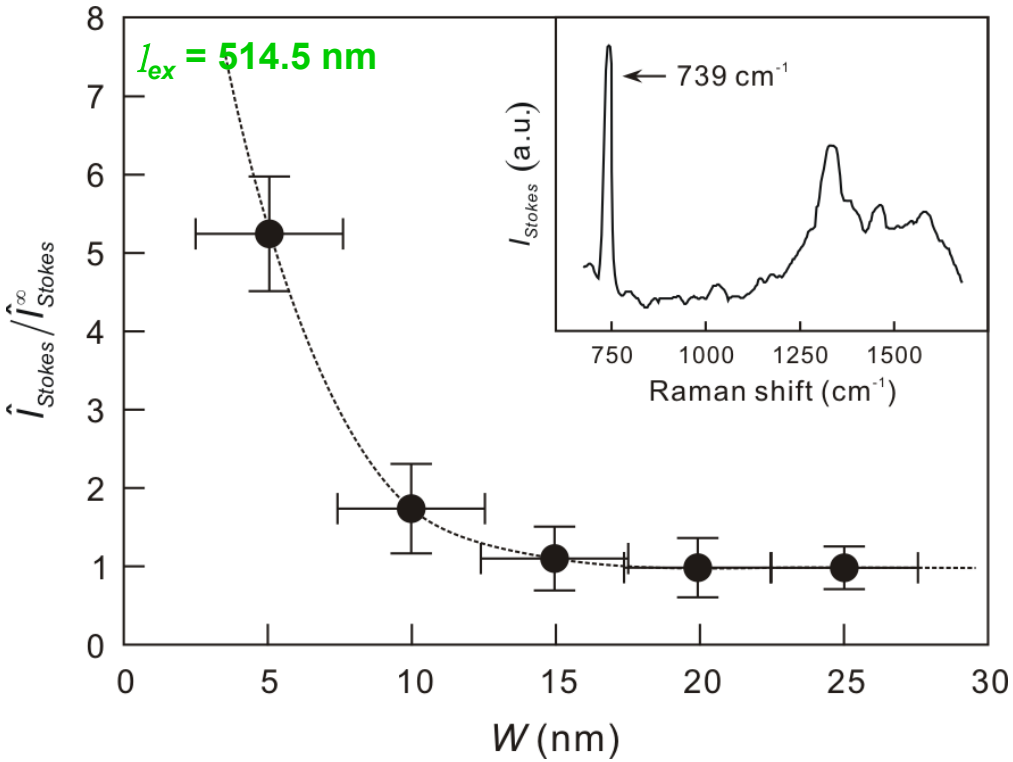

H.-H. Wang et al., Adv. Mater. 18, 491 (2006).

Plasmonic coupling in far-field optical properties

- Two questions emerge: (1) How is the plasmonic coupling within these hot spots reflected in far-field optical measurements? (2) How is the dependence on interparticle spacing understood quantitatively?
- Though there exist many experimental studies, only qualitative understanding has been provided.[1] They are limited by the use of large disk-shaped nanoparticles made by electron-beam lithography[1] or complex sculpted structures made by nanosphere lithography. The complex geometry of these nanostructures renders the interpretation of the spectra rather difficult, if not impossible.
- Several theoretical efforts have been made to reveal the intricate electromagnetic interaction between near-by nanoparticles.[2] A comprehensive analytic model to interpret experimental observations is still missing.

[1] *For example, K.-H. Su et al., Nano. Lett. 3, 1087 (2003); P. K. Jain et al., Nano. Lett. 7, 2080 (2007).*

[2] *B. N. J. Persson et al., Phys. Rev. B 28, 4247 (1983); V. A. Markel, J. Mod. Opt. 40, 2281 (1993).*

Ag nanoparticle arrays grown in AAO

Dr. Juen-Kai Wang, CCMS, NTU

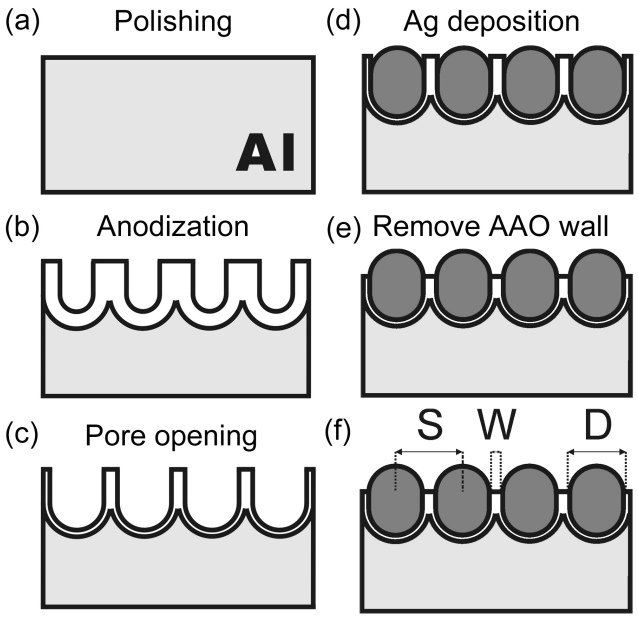

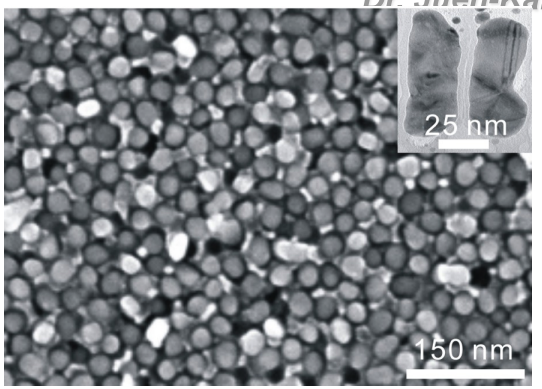

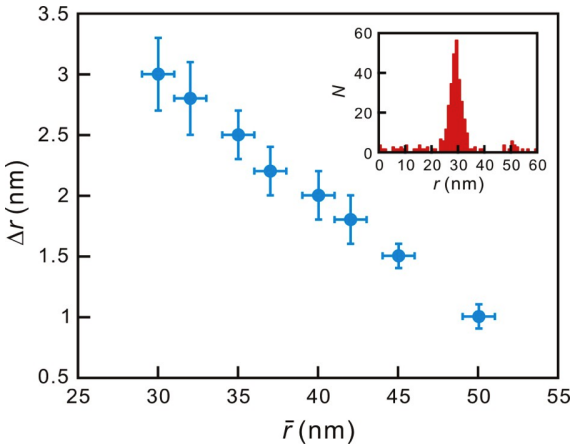

- The minimum interparticle spacing is 30 nm, corresponding to a gap of 5 nm.
- The standard deviation width of the distribution of the interparticle spacing, Δr, decreases monotonically with the mean interparticle spacing, $\bar{r}$.

H.-H. Wang et al., Adv. Mater. 18, 491 (2006); S. Birin et al., Opt. Exp. 16, 15312 (2008).

Scattering spectrum *vs*. interparticle spacing

Dr. Juen-Kai Wang, CCMS, NTU

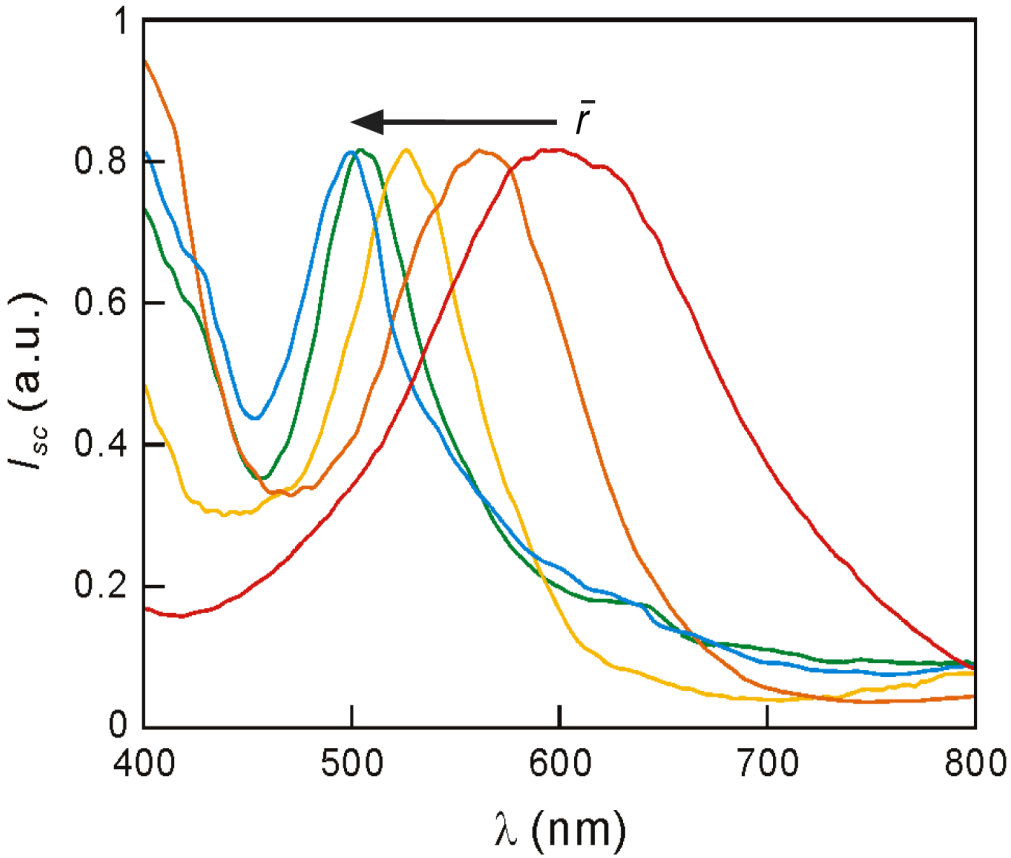

- The resonance peak is red-shifted and the resonance width is broadened as the interparticle spacing, $\bar{r}$, decreases.

S. Birin et al., Opt. Exp. 16, 15312 (2008).

Hexagonal nanoparticle array

Dr. Juen-Kai Wang, CCMS, NTU

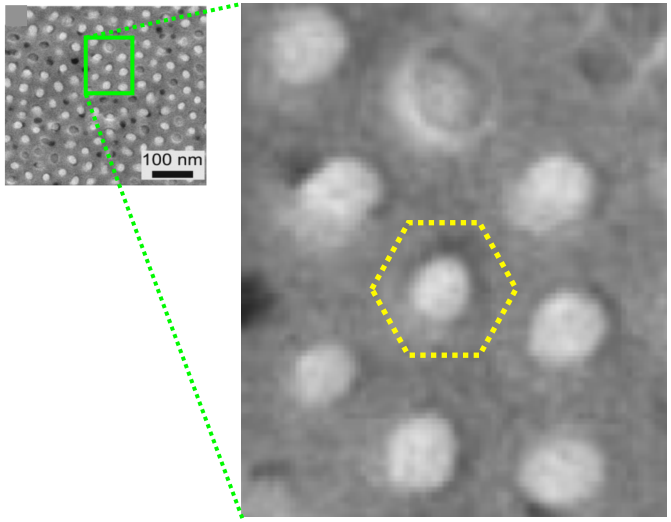

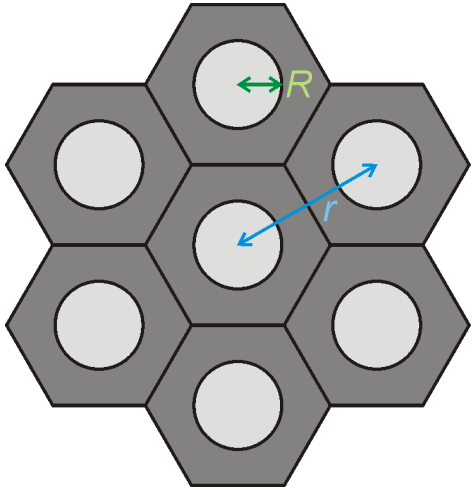

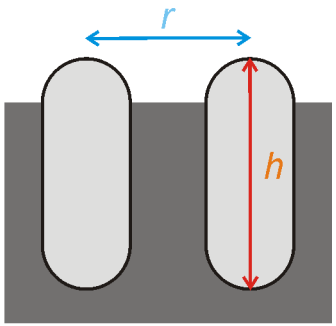

- The Ag nanoparticle arrays can be considered as two-dimensional hexagonal arrays made of Ag prolate spheroids in AAO matrix.

S. Birin et al., Opt. Exp. 16, 15312 (2008).

Polarizability of single Ag nanoparticle

Dr. Juen-Kai Wang, CCMS, NTU

- Transverse-mode polarizability of single prolate spheroid along its short axis[1] (quasi-static dipole model)

$$\alpha_T(\omega) = R^2 h \frac{\varepsilon(\omega) - \varepsilon_m}{3\varepsilon_m + 3L\left[\varepsilon(\omega) - \varepsilon_m\right]} \qquad L = \frac{1}{2} - \frac{1-e^2}{2e^2}\left(-1 + \frac{1}{2e}\ln\frac{1+e}{1-e}\right) \qquad e^2 = 1 - (R/h)^2$$

e_m: dielectric constant of the surrounding medium; *R*: the radius; *h*: the length

- Drude model

$$\varepsilon(\omega) = 1 - \frac{\omega_p^2}{\omega(\omega + i/\tau)}$$

w_p: plasma frequency; t: relaxation time

- Transverse-mode polarizability of single Ag prolate spheroid

$$\alpha_T(\omega) \approx \left(\frac{S^3}{1 + C\varepsilon_m}\right)\left[(\varepsilon_m - 1)\omega^2 + \omega_p^2\right] \Big/ \left(\frac{\omega_p^2}{1 + C\varepsilon_m} - \omega^2 - i\frac{\omega}{\tau}\right) \qquad w_p >> t$$

$$S^3 = R^2 h / 3L \qquad C = (1 - L)/L$$

[1] *C. F. Bohren and D. R. Huffman, Absorption and Scattering of Light by Small Particles (Wiley, New York, 1983), p. 130.*

Self-consistent electromagnetic interaction theory

Dr. Juen-Kai Wang, CCMS, NTU

- Local electric field at each dipole in a dipole array

$$\boldsymbol{E}_{loc}(\boldsymbol{r}_i)=\boldsymbol{E}_{inc}(\boldsymbol{r}_i)+\sum_{j\neq i}\frac{e^{ikr_{ij}}}{r_{ij}^3}\left[k^2\boldsymbol{r}_{ij}\times(\boldsymbol{r}_{ij}\times\boldsymbol{P}_j)+\frac{1-ikr_{ij}}{r_{ij}^2}\times\left\{r_{ij}^2\boldsymbol{P}_j-3\boldsymbol{r}_{ij}(\boldsymbol{r}_{ij}\cdot\boldsymbol{P}_j)\right\}\right] \qquad \boldsymbol{P}_i=\alpha_T\boldsymbol{E}_{loc}(\boldsymbol{r}_i)$$

- Effective polarizability of a dipole in an dipole array[1]

$$\alpha_{eff}=\frac{\alpha_T}{1-\alpha_T U} \qquad U=\sum_{j\neq i}\left[\underbrace{\frac{k^2\sin^2\theta_{ij}}{r_{ij}}}_{\text{Far-zone term}}-\underbrace{\frac{ik\left(3\cos^2\theta_{ij}-1\right)}{r_{ij}^2}}_{\text{Intermediate-zone term}}+\underbrace{\frac{\left(3\cos^2\theta_{ij}-1\right)}{r_{ij}^3}}_{\text{Near-zone term}}\right]e^{ikr_{ij}}$$

q_{ij}: the angle between $\boldsymbol{r}_{ij}$ and $\boldsymbol{E}_{inc}$

- Derivation of a_{eff}

$$\alpha_{eff}=\frac{S^3\left[(\varepsilon_m-1)\omega^2+\omega_p^2\right]}{\left[\left(1-S^3A\right)\omega_p^2-\left\{(1+C\varepsilon_m)+(\varepsilon_m-1)S^3A\right\}\omega^2\right]-i\left[(\varepsilon_m-1)S^3B\omega^2+(1+C\varepsilon_m)(\omega/\tau)+S^3B\omega_p^2\right]}$$

$$U=A+iB \qquad U\approx F\cdot r^{-3}+iB \qquad B=\sum_{j\neq i}\left(3\cos^2\theta_{ij}-1\right)\left[\sin\left(kr_{ij}\right)r_{ij}^{-3}-k\cos\left(kr_{ij}\right)r_{ij}^{-2}\right]$$

[1]B. N. J. Persson and A. Liebsch, Phys. Rev. B 28, 4247 (1983); S. Birin et al., Opt. Exp. 16, 15312 (2008).

Spectroscopic properties of EM scattering

Dr. Juen-Kai Wang, CCMS, NTU

- Resonance peak

$$\Omega_T^2 = \frac{\omega_p^2\left[1 - F\left(S/r\right)^3\right]}{\left(1 + C\varepsilon_m\right) + \left(\varepsilon_m - 1\right)F\left(S/r\right)^3}$$

- Resonance width

$$\Gamma = \frac{1}{\tau} + \frac{S^3 B\omega_p^2}{\left(1 + C\varepsilon_m\right)\Omega_T} + \frac{\varepsilon_m - 1}{1 + C\varepsilon_m} S^3 B\Omega_T$$

- Scattering intensity

$$I\left(\Omega_T\right) \propto N\left(r\right)\Omega_T^4 \left|\alpha_{eff}\left(\Omega_T\right)\right|^2 = N\left(r\right)\left\{\frac{\Omega_T S^3\left[\left(\varepsilon_m - 1\right)\Omega_T^2 + \omega_p^2\right]}{\Gamma\left(1 + C\varepsilon_m\right)}\right\}^2$$

- The extra contribution in the resonance width is proportional to *B* which is Im(*U*).

S. Birin et al., Opt. Exp. 16, 15312 (2008).

Resonance peak and width

Dr. Juen-Kai Wang, CCMS, NTU

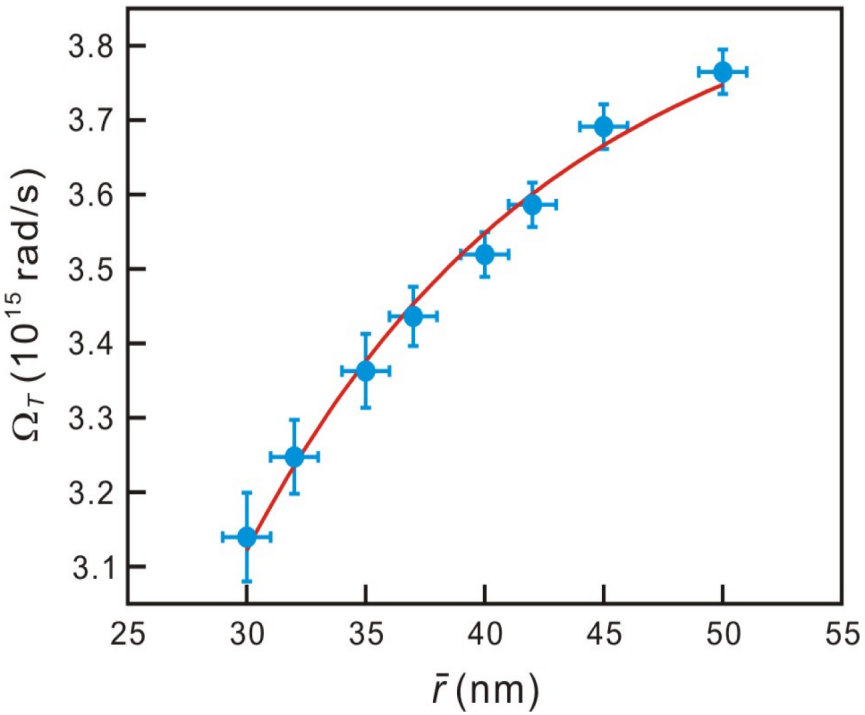

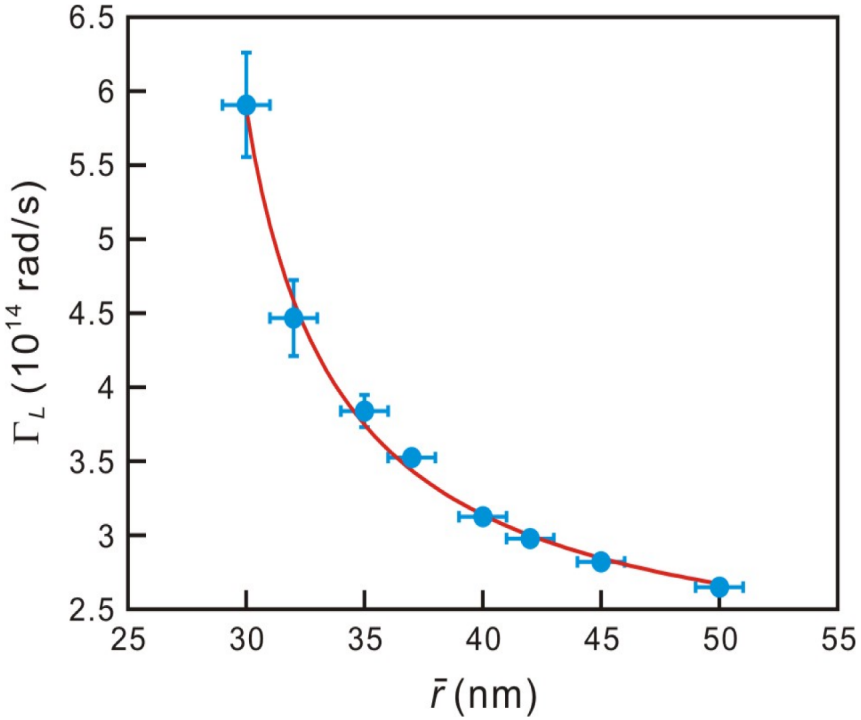

- The spectral shape is fitted to a Voigt profile to extract its resonance peak (Ω_T) and Lorentzian width (Ω_L) with the use of the distribution of the interparticle spacing.
- The dependences of Ω_T and Ω_L on the mean interparticle spacing, $\bar{r}$, agree well with the theoretical prediction.

S. Birin et al., Opt. Exp. 16, 15312 (2008).

High accuracy calculation with PSTD method

Dr. Juen-Kai Wang, CCMS, NTU

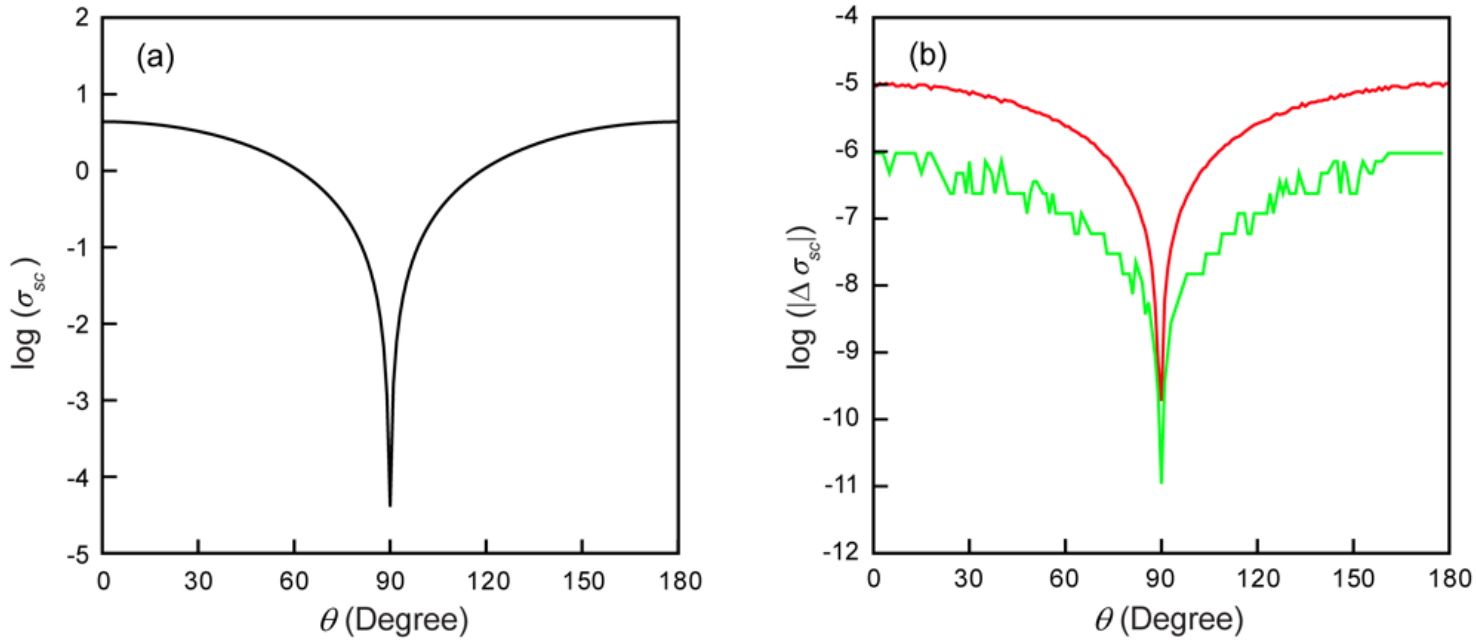

- A multi-domain pseudospectral computational framework in time domain, so called pseudo-spectral time-domain (PSTD) method, is adopted for calculation.
- **Errors in Mie scattering problem**: The calculation error for an silver sphere in scattering cross section at resonance wavelength is less than 10^{-6} and the corresponding near-field error is less than 3×10^{-3}, which are much smaller than that based on discrete-dipole approximation (DDA) and finite-difference time-domain (FDTD) methods (near-field error > 2%).

C.-H. Teng et al., J. Sci. Comput. 36, 351 (2008).